Competition between Chiral Energy and Chiral Damping in the Asymmetric Expansion of Magnetic Bubbles

Arnab Ganguly, Senfu Zhang, Ioan Mihai Miron, Jürgen Kosel, Xixiang Zhang, Aurelien Manchon, Nirpendra Singh, Dalaver Anjum, Gobind Das

▶ **To cite this version:**

Arnab Ganguly, Senfu Zhang, Ioan Mihai Miron, Jürgen Kosel, Xixiang Zhang, et al.. Competition between Chiral Energy and Chiral Damping in the Asymmetric Expansion of Magnetic Bubbles. ACS Applied Electronic Materials, 2021, 3 (11), pp.4734-4742. 10.1021/acsaelm.1c00592 . hal-03831772

HAL Id: hal-03831772
https://hal.science/hal-03831772v1

Submitted on 27 Oct 2022

HAL is a multi-disciplinary open access archive for the deposit and dissemination of scientific research documents, whether they are published or not. The documents may come from teaching and research institutions in France or abroad, or from public or private research centers.

L'archive ouverte pluridisciplinaire **HAL**, est destinée au dépôt et à la diffusion de documents scientifiques de niveau recherche, publiés ou non, émanant des établissements d'enseignement et de recherche français ou étrangers, des laboratoires publics ou privés.

Competition between chiral energy and chiral damping in the asymmetric expansion of magnetic bubbles

Arnab Ganguly[1,2§], Senfu Zhang[1], Ioan Mihai Miron[3], Jürgen Kosel[1], Xixiang Zhang[1], Aurelien Manchon[1,4*], Nirpendra Singh[2] Dalver H. Anjum[2] and Gobind Das[2*]

[1] Physical Science and Engineering Division, King Abdullah University of Science and Technology, Thuwal 23955-6900, Saudi Arabia.

[2]Department of Physics, Khalifa University, Abu Dhabi 12788, United Arab Emirates.

[3]CNRS, SPINTEC, 38000 Grenoble, France.

[4]CINaM, Aix-Marseille University, CNRS, Marseille, France.

*Corresponding email: manchon@cinam.univ-mrs.fr, gobind.das@ku.ac.ae

§ Present address: Department of Physics, Khalifa University, Abu Dhabi 12788, United Arab Emirates.

Abstract

Magnetic chirality is an important knob in spintronics and can be engineered through structural symmetry breaking of magnetic thin film multilayers. The dynamics of chiral domain walls is determined by the cooperation of chiral contributions in the magnetic energy functional as well as in the dissipation tensor which need to be better controlled for the sake of the device applications. In this work, we performed a systematic study of magnetic field-induced magnetic bubble expansion in structural inversion asymmetric multilayers with different Pt thicknesses using polar magneto-optical Kerr microscopy. Asymmetric expansion of magnetic bubble is investigated in the creep regime as a function of in-plane and out-of-plane magnetic fields. The results reveal the competition between two key mechanisms governing the asymmetry in the field-driven domain wall expansion, namely the Dzyaloshinskii-Moriya interaction and the chiral magnetic damping. The interplay between these two effects leads to seemingly counterintuitive experimental signature, depending on the strength of the external magnetic field. The effective control on the

bubble asymmetry expansion can be of great importance for the future memory and multiplexer based applications.

Keywords: chiral damping, Dzyaloshinskii-Moriya interaction, magnetic bubble expansion

Magnetic domains are candidate building blocks for modern long-term magnetic data storage[1-3]. The out-of-plane magnetic domains with switchable magnetization direction are commonly used as binary memory bits for non-volatile devices[4-6]. The ultrahigh mobility of current-driven magnetic domain walls recently observed in non-centrosymmetric heterostructures[7-9] opening attractive opportunities for alternative storage and data transfer technologies such as the magnetic racetrack[1,10]. Hence, a precise understanding of the physical characteristic of the dynamics of magnetic domain walls in such heterostructures can substantially enhance the magnetic devices performance [11-15]. The typical system (e.g., $Pt/Co/AlO_x$) consists of a perpendicularly magnetized thin film embedded between dissimilar heavy metals shows current-driven high domain wall velocity up to 400 m/s [7,8]. The high velocity is attributed to the cooperation between damping-like torque arising from the adjacent heavy metals and Dzyaloshinskii-Moriya interaction (DMI) present at the interfaces[16,17]. The magnitude of the damping-like torque is normally assessed through spin-torque or spin-pumping measurements[18-20], while magnitude of the DMI is determined by the following ways. Various imaging techniques such as Nitrogen vacancy centers magnetometry[21-23], scanning transmission X-ray microscopy[24], electron or X-ray holography[25-28], and Lorentz microscopy[29-32] allow for direct observation of the chirality of the domain wall, confirming that interfacial DMI favors Néel configuration over Bloch configuration[33]. Brillouin light scattering[34-36] determines the momentum shift of counter-propagative spin waves through inelastic scattering. Finally, several methods have been proposed based on the dynamical characteristics of the domain wall motion. In the simplest model, DMI translates into an effective in-plane magnetic field, which can be determined by recording the velocity shift obtained when applying an external field or probing the asymmetric expansion of magnetic bubbles[37-41]. The asymmetric expansion in the magnetic bubble is driven by a small external magnetic field in the creep regime, *i.e.*, a regime of motion dominated by thermal activation in the presence of a considerable disorder. However, the creep motion is a subtle regime of motion where energy dissipation plays a crucial role. Herein, we propose the symmetry breaking of the system translate into the emergence of a chiral contribution to the magnetic damping. To date, it remains unclear how DMI (chiral energy) and chiral damping compete with each other in the context of creep motion. In this article, we perform a systematic study of field and current-induced domain wall motion in multilayers with inversion symmetry breaking. We also suggest that both effects (DMI and chiral damping) display quite different domain-velocity dependency on

materials. As such, we propose that the asymmetric expansion of the magnetic bubble is dominated by either DMI or chiral damping in opposite limits.

Results

Thin film multilayer of Ta(3 nm)/Pt(3 nm)/Co (0.6 nm)/Pt (d_{Pt})/IrMn(3 nm) is deposited using dc/rf magnetron sputtering. Here, d_{Pt} varies from 0 to 1 nm for field induced and 0 to 5 nm for current induced domain wall motion studies. The thin film stack, along with the experimental configuration, is illustrated in fig. 1(a). The sputtering conditions are carefully chosen to obtain perpendicular magnetic anisotropy in these films. The experiment is performed using magneto-optical Kerr effect microscopy in polar geometry[42-45]. A differential Kerr imaging is performed to observe the magnetic domains and to eliminate the contribution of any nonmagnetic intensities. Square pulses of the magnetic field are applied both in-plane and out-of-plane of the sample using two independent electromagnets. To nucleate a bubble, the thin film magnetization is saturated in one perpendicular direction followed by an out-of-plane field pulse in the opposite direction. The bubbles nucleate from defects or pinning centers present in the sample. The in-plane magnetic field (H_x) alone cannot nucleate or drive bubbles because of strong perpendicular magnetic anisotropy (PMA) of the sample but it induces asymmetric motion when combined with the out-of-plane field (H_z). For proper synchronization and temporal overlap between the fields, the in-plane pulse is chosen longer than the out-of-plane pulse.

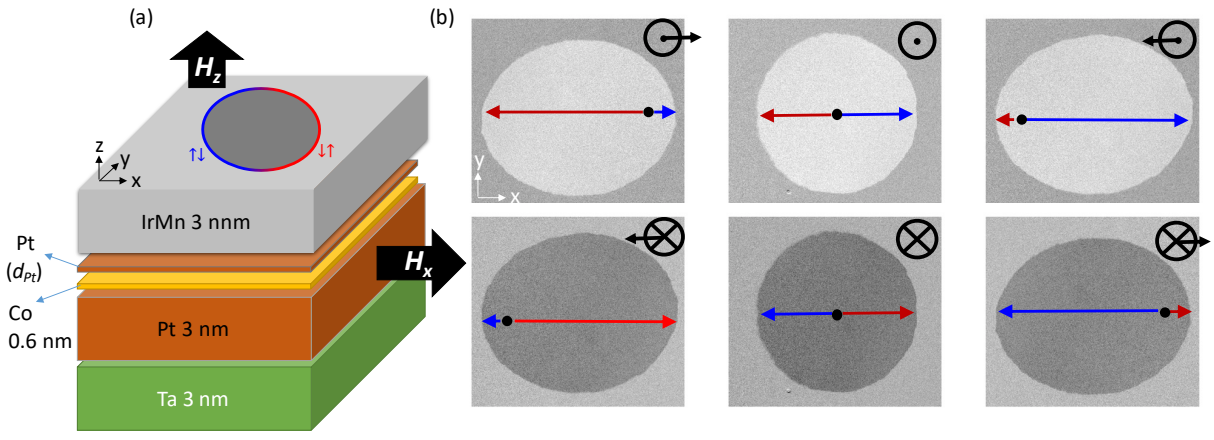

Figure 1: (a) Schematic illustration of sample along with the field configuration of bubble expansion experiment. (b) Kerr microscopy images of magnetic bubbles at different field orientations. The

orientation for the H_x and H_z are denoted in the top right corner of each figure. Red and blue arrows indicate the propagation of opposite domain walls from the nucleation center.

Asymmetric bubble expansion.

Figure 1(b) shows differential Kerr images of magnetic bubbles in Ta(3 nm)/Pt(3 nm)/Co(0.6 nm)/IrMn(3 nm) under six different field configurations. The dark and bright contrasts in this image indicate ↓ and ↑ out-of-plane configuration of the magnetization vector. Red and blue arrows indicate the expansion of ↓↑ and ↑↓ domain walls while the black dot between the arrows indicates the nucleation center of the bubbles. Here, a 15 ms long out-of-plane field pulse (H_z =120 Oe) is applied for the expansion of the bubbles. The direction of H_z is shown at the top right corner of each image. An additional in-plane field (H_x=2 kOe) is applied in some cases as indicated in the top right corner of the figures.

We observe that without an in-plane field the bubbles are circular or symmetric with respect to origin. In the presence of an in-plane field, the velocities of ↓↑ and ↑↓ domain walls are very asymmetric along x-direction. The asymmetry changes sign with the reversal of H_x. This asymmetry can be originated in two ways. In the widely accepted scenario, the presence of DMI creates an effective in-plane magnetic field, normal to the domain wall, and favors the Néel configuration[46]. An external magnetic field lowers the energy of one side of the bubble with respect to the other (in one case, Néel wall is enforced, while it is weakened in the other), resulting in an asymmetric creep expansion. Another scenario is possible, though, and does not necessitate the presence of a DM field. If no such field is present, magnetostatics dictates that the magnetic moments at the bubble boundary adopt a Bloch configuration. Applying an in-plane magnetic field therefore promote Neel configuration. Thus, the two opposite sides of the bubble adopt the opposite chirality. If the magnetic damping is sensitive to this chirality[47], then the opposite sides of the bubble are expected to dissipate energy differently, resulting in a different creep velocity and, thereby, an asymmetric expansion. As a general rule, one expects that both effects should coexist, and till now, it remains unclear how to distinguish them. To do so, we analyze the dependence of the velocity of the bubble boundary as a function of the in-plane and out of plane field.

In-plane field dependence of domain wall velocity

The variation of domain wall velocities with in-plane field is studied in this section. Figure 2(a-f) shows velocities for ↓↑ and ↑↓ domain walls by red and blue curves plotted on the left side and velocity asymmetry ($A = 2(v_{\downarrow\uparrow} - v_{\uparrow\downarrow})/(v_{\downarrow\uparrow} + v_{\uparrow\downarrow})$) on the right side of each figure. The thickness of top Pt, d_{Pt} is indicated on each figure. Figure 2(a)-left shows that for d_{Pt} =0, the velocity of ↓↑ domain walls (red curve) is larger than that of ↑↓ domain walls (blue curve) at positive in-plane field. Moreover, the former increases with the field value whereas the latter decreases with it. At negative field, we have the opposite scenario. All the curves in Fig. 2 are symmetrically opposite with respect to zero field as the sample does not have any preferential direction. On the right side of Fig. 2(a), the velocity asymmetry A changes sign from positive to negative as the field is reversed from positive to the negative direction. The magnitude of A increases faster at lower field and slows down at higher field, although saturation is not observed until 3 kOe. In Fig. 2(b) for d_{Pt} =0.2 nm the velocity of the ↑↓ wall (blue curve) starts to increase after a critical field H_C = +2 kOe thus causing a slope reversal in the blue curve as well as in the A curve around the same region (indicated by arrows). At d_{Pt} =0.3 nm the feature is observed at a lower field of H_C ~1.5 kOe [Fig. 2(c)]. The velocity of the ↑↓ wall (blue curve) starts increasing dramatically after H_C, and overtakes the ↓↑ wall velocity (red curve) at 2 kOe. In this case, A changes sign for the same sign of H_x across 2 kOe. For d_{Pt} =0.5 and 0.7 nm, H_C is around 0.5 and 0.2 kOe and finally at d_{Pt}=1 nm the value is close to zero [Fig. 2(d-f)]. In Fig. 2(f) (d_{Pt}=1 nm) the velocity of ↑↓ wall (blue curve) is much higher than that of the ↓↑ wall (red curve) at positive field. The asymmetry is opposite as compared to Fig. 2(a) (d_{Pt}=0 nm). Apart from that, another contrast between Figs. 2(a) and 2(f) is the saturation field of asymmetry curves. In the first case no saturation is observed until 3 kOe while in the second case it occurs ~1.2 kOe. The shape of the velocity curves for d_{Pt}=0 and 1 nm are completely different. In the former case it is exponential and in the latter case it is linear. From these observations it appears that there is a competition between two effects responsible for the velocity asymmetry, one dominating at lower values of d_{Pt} and the other at higher values of d_{Pt}. The chiral contribution to the magnetic energy, i.e., the DMI contribution, can be viewed as an internal in-plane field acting on the domain wall, a change of which causes an opposite lateral shift of in-plane velocity curves for the two opposite walls. Any feature in the velocity curve thus gets laterally shifted and manifested at different field but at same velocity. The chiral contribution to energy dissipation, i.e. the chiral damping, does not impact the magnetic energy itself, rather the

attempt frequency controlling the thermal activation[12,40]. This gets the velocity curves shifted vertically in opposite directions, thus the feature manifested at same field but at different velocities[40]. In Fig. 2(a), H_C is out of the measurement range and from Figs. 2(b) to (f) H_C monotonically decreases close to zero value. This suggests that for d_{Pt} =0, we have the highest internal DMI field which progressively vanishes upon increasing the top Pt layer thickness. The observation is consistent with previous literature showing that DMI arising from opposite interfaces tend to cancel each other[38,48]. The exponential variation of the velocity curve in Fig. 2(a) also supports that the asymmetry is coming from energy. In Fig. 2(c) opposite asymmetry is observed across 2 kOe for the same applied field direction as the asymmetry curve crosses the zero line. A mere decrease internal DMI field cannot explain this phenomenon. Indeed, in such case the sign of A would remain the same for a particular direction of H_x This unconventional sign reversal process suggests that a completely different mechanism takes over the DMI field upon increasing d_{Pt}. This mechanism is attributed to chiral damping, eventually dominating over the internal DMI field which will be discussed in the later part of the paper. This argument is also supported by the non-exponential velocity curve in Fig. 2(f) that strongly differ from the more exponential dependence observed in Fig. 2(a).

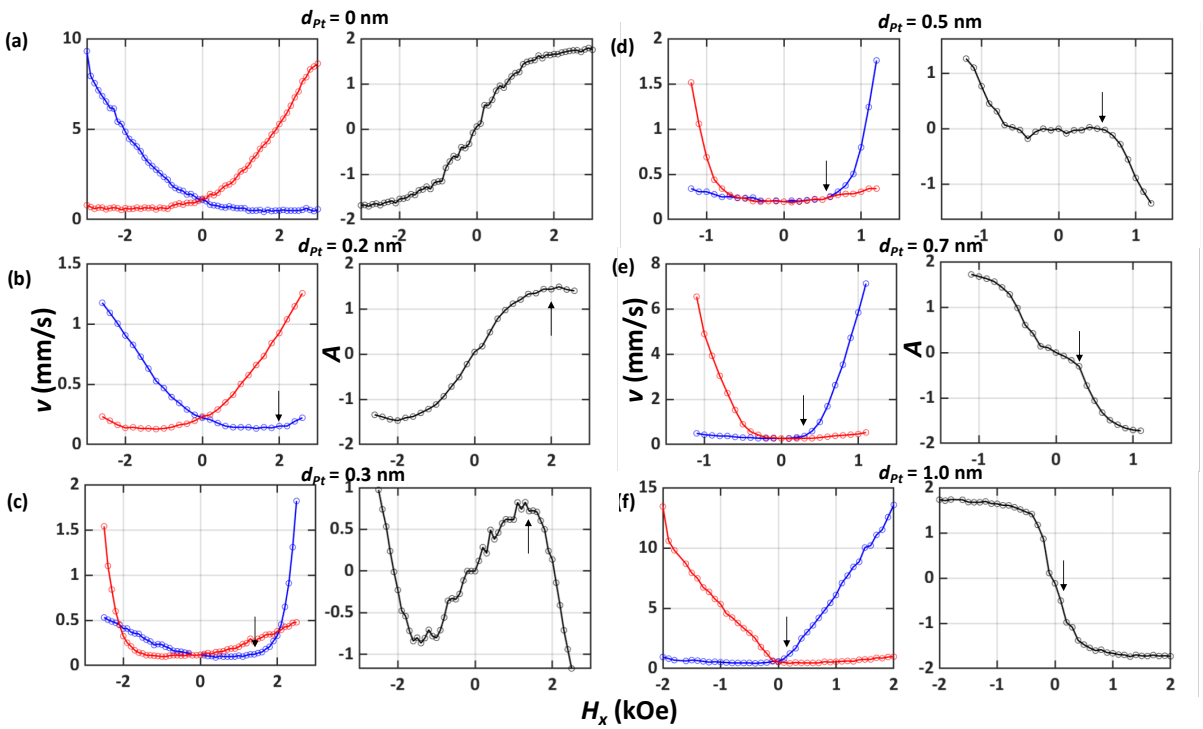

Figure 2: (a-f: left) In-plane field dependent velocity curves of ↓↑ (red) and ↑↓ (blue) domain walls and (a-f: right) corresponding velocity asymmetry for top Pt thicknesses of d_{Pt} =0, 0.2, 0.3, 0.5, 0.7 and 1 nm.

To estimate the values of DMI field and its dependence upon increasing top Pt thickness, current-induced domain wall motion has been studied in presence of in-plane magnetic field. Thin film micro strips are fabricated using photo-lithography. A transverse domain wall is created on the strip. Simultaneous current and in-plane magnetic field pulse are applied along the length of the film. The current drives the domain wall while the in-plane field either helps or opposes the propagation by favoring one Néel chirality over the other, depending on the direction of the field. Thus, there exists a compensating field H_x for which the current-induced domain wall velocity vanishes. In that case, the applied field completely opposes the internal DMI field. Thus by measuring the compensation field we extract the DMI field value of the film. Figure 3(a) shows velocity curve as a function of in-plane field for a constant current density. In our experiment a ↓↑ domain wall is driven by current pulses from the left. A field parallel (antiparallel) to the current direction is considered positive (negative). For all different values of d_{Pt}, the domain wall velocity changes exponentially with field. In each of the cases, there is a field range for which the velocity of the domain wall is zero and there exists two avalanche fields (H_{av}) in either side of which domain wall starts to move either along or opposite to the current direction, respectively. It is found that with increasing current density both the H_{av}'s converge to their mean value. That means that the mean value of H_{av} does not change with current density which is nothing but the DMI field (H_D) of the sample. At lower current density the error associated with H_D is larger because of the flatness of the curve. On the other hand, at higher current density the probability of nucleation of other domains masking the domain wall of interest increases. Hence, practically the experiment is limited to a certain current density and the corresponding error on H_D. The estimated H_D is plotted in Fig. 3(b) as a function of the Pt thickness. The experiment confirms the DMI changes sign at d_{Pt} =3 nm. From d_{Pt} =0 to 1 nm the DMI field decreases but does not change sign to cause opposite asymmetry as observed in Fig. 2. This observation confirms the scenario of the two distinct competing mechanisms.

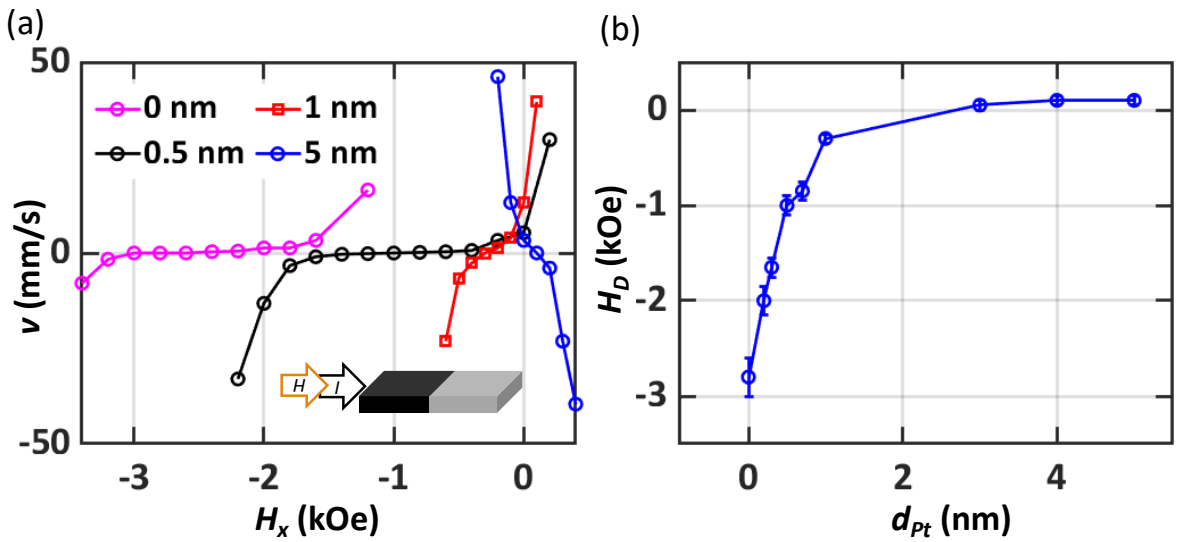

Figure 3: (a) In-plane field dependent ↓↑ domain wall velocity. Inset shows the positive current and field convention. (b) The DMI field estimated as a function of top Pt thicknesses.

Out-of-plane field dependence of domain wall velocity

In the previous part, we have discussed asymmetric domain wall motion on qualitative grounds, avoiding entering into the details of the motion regime. General arguments based on the global behavior of the velocity asymmetry led us to postulate the competition between two chiral mechanisms. Let us now provide a more quantitative analysis of these two effects, based on the specific motion regime experienced by the domain wall. In our experiments, the domain wall moves in the thermally activated creep regime. Recent literature by Jué *et al.*[40] show that the velocity of domain wall in the creep regime can be modeled by creep scaling law as

$$v = (d_0 f_0).e^{\left[\frac{-U_C(H_P)}{K_B T}\left(H_z^{-\frac{1}{4}} - H_o^{-\frac{1}{4}}\right)\right]} \quad (1)$$

Where, $H_o = H_P/C^4$ ($C \sim 1$ is an empirical constant) and d_0, f_0, H_P, and U_C are the disorder correlation length, de-pinning attempt frequency, pinning field and pinning barrier respectively. In the exponent, the energy barrier $U_c(H_P)$ accounts for non-dissipative processes described by the magnetic energy functional. In particular, DMI is one such energy process that is discussed in previous literatures as a factor for controlling the asymmetry of the domain wall velocity[41,48-51]. On the other hand, f_0 is inversely proportional to the energy dissipation[52] In other words, a

change in the exponential coefficient reflects a change in the energy functional while a change in the pre-factor indicates a change in the energy dissipation of the system. When the logarithmic velocity is considered with respect to $H_z^{-1/4}$, the curve is linear in the creep regime with a change in slope indicating change in the energy and vertical shift representing change in the dissipation.

In Fig. 4(a-f), logarithmic velocities are plotted with varying out-of-plane field for different top Pt layer thicknesses as mentioned in each figure. The variation is well fitted by straight lines with negative slope (m) confirming that our measurement is in the creep regime. Each velocity curve is measured in presence of a constant H_x indicated next to the curve in Fig. 4a. For each in-plane field, the velocity is measured for ↓↑ and ↑↓ domain walls, reported in red and blue color, respectively. In general, the velocity curves in Fig. 4 are approximately parallel or make a small angle with each other. For d_{Pt}=0 [Fig. 4(a)], when an in-plane field is applied along x, the ↓↑ domain wall velocity slope (red curves) is shifted up to higher velocity while the ↑↓ domain wall velocity slope (blue curves) moves down to lower velocity side with respect to zero field curve. In the other cases [Fig. 4(b-f)], when top Pt layer is introduced, H_x causes a positive shift for *both* ↓↑ and ↑↓ curves. With increasing Pt thickness the ↑↓ (blue) curves experience a dramatic vertical shift achieving higher velocity while the shift for the ↓↑ (red) curves remains very small. This suggests that the chiral damping mechanism, present in the prefactor of Eq. (1), gets activated with the insertion of Pt assisting the ↑↓ (blue) domain wall to move faster than ↓↑ (red) walls and thus altering the asymmetry.

In order to provide a synthetic picture of the overall behavior of the velocity asymmetry, Fig. 4(g) displays $\delta m = (m_r - m_b)$, the difference between the slope of the velocity of ↓↑ (red) and ↑↓ (blue) walls as a function of H_x. The colors indicate different values of d_{Pt}.as indicated next to each curve The curves are fitted by the phenomenological formula $a(e^{-bH_x} - 1)$ where a and b are constants denoting the amplitude and saturation of the curve. From Fig. 4(g), it is found that the saturation field decreases with Pt thickness very similar to Fig. 3(b). Here the saturation essentially means that the energy difference between the opposite domain walls saturates at a field equal to the DMI field of the sample. As the DMI field decreases with Pt thickness the saturation field decreases. Figure 4(h) shows the vertical shift of the velocity curves in Fig. 4(a-f) with respect to H_x=0 curve at constant fields [H_x=1.5 kOe and $\mu_0 H_z$=0.55 (mT)$^{-1/4}$]. As mentioned above, the asymmetry in the vertical shift is attributed to the chiral contribution in the prefactor of Eq. (1),

i.e., to chiral damping. It is found that the ↑↓ (blue) curves get monotonically shifted to higher velocity with Pt thickness while for ↓↑ (red) curves the shift is significantly smaller and weakly depends on the Pt thickness. This suggests that the chiral damping mechanism gets activated with the insertion of Pt assisting the ↑↓ (blue) domain wall to move faster than the ↓↑ (red) one and thus altering the asymmetry. It is intriguing to observe that ↑↓ and ↓↑ domain walls are affected differently by the chiral damping.

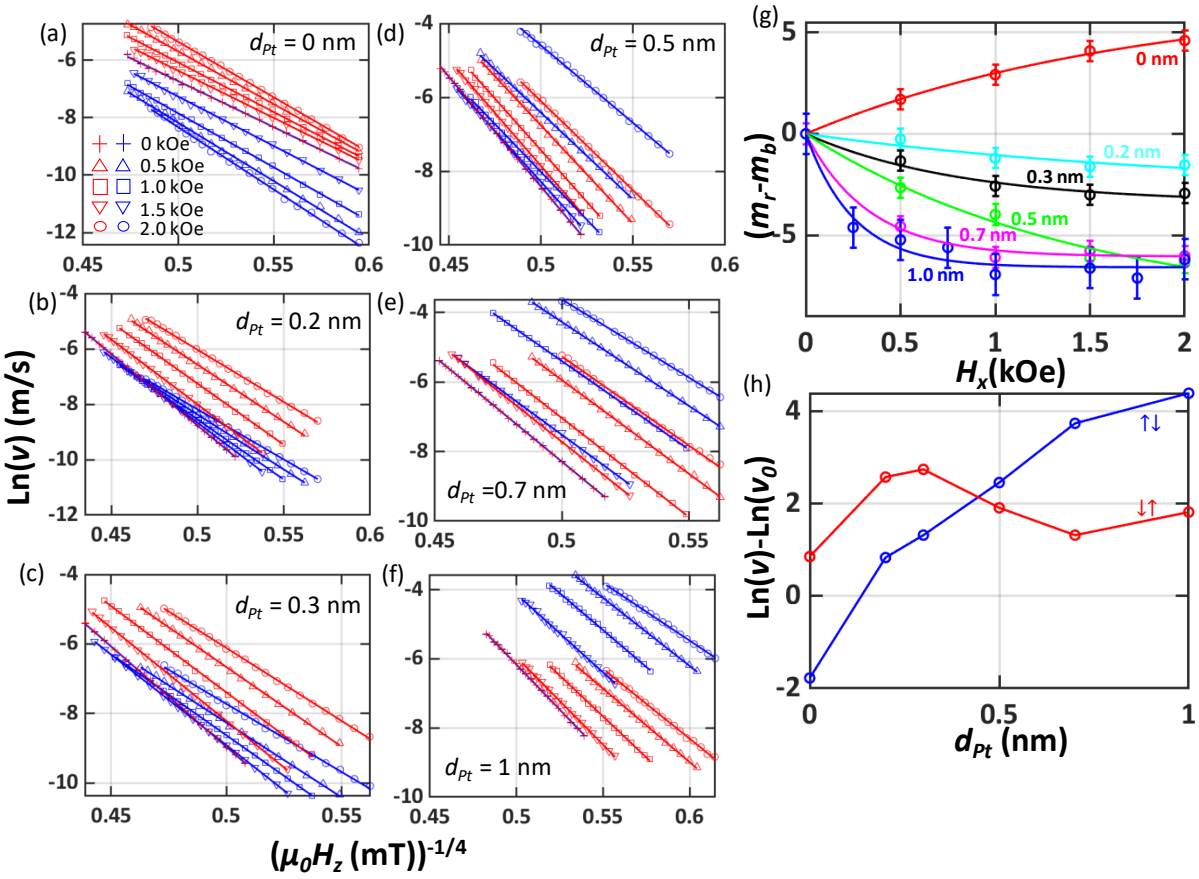

Figure 4: (a-f) out-of-plane field dependence of the logarithmic velocity of bubble domain. The scattered points are experimentally observed data while the straight lines are the fitted data. The red and blue lines correspond to ↓↑ and ↑↓ domain wall velocities (g) The slope difference for the opposite domain walls obtained from fig. 4(a-f) as a function of in-plane field and (h) velocity shift for the red and blue domain walls with respect to H_x=0 for different Pt thicknesses.

The analysis of current-driven motion (Fig. 3) and field-driven motion (Fig. 4) confirm the competition of two chiral mechanisms that we interpret at DMI field and chiral damping, which dominate at different Pt thicknesses. In Fig. 5, the asymmetry curves reported in Fig. 2 are fitted using the DMI and chiral damping models. From the very definition two distinct asymmetry curves can be identified as at a large field asymmetry reduces close to zero in case of DMI while it saturates in case of chiral damping. The domain wall velocity asymmetry due to DMI is represented by $v = v_0 e^{c|H_x + H_D|}$ and the asymmetry by $A_{DMI} = 2\frac{v_{\downarrow\uparrow} - v_{\uparrow\downarrow}}{v_{\downarrow\uparrow} + v_{\uparrow\downarrow}}$. The chiral damping asymmetry is characterized by a phenomenological saturation function $A_{CD} = 2\left(1 - e^{-\frac{H_x}{s}}\right)$, s being a parameter related to the saturation. Both the asymmetries are multiplied by a weight factor to consider their relative contribution to the overall asymmetry. All the asymmetry curves are well fitted by a combination of these two effects with H_D as a fixed parameter extracted from the current-induced experiment in Fig. 3. The purple shade of each figure denotes the DMI contribution while the green shade indicates the chiral damping contribution. From Fig. 5 we see that both curves are symmetrically opposite which means that chiral damping and DMI compete with each other. From Fig. 5(a) to (f) we see that the DMI contribution decreases progressively when increasing Pt thickness, while the chiral damping contribution increases. Figure 5(g) displays the ratio between the chiral damping and DMI contributions to the asymmetry, as obtained from Fig. 5(a-f). It clearly indicates that chiral damping steadily increases over DMI upon increasing the Pt thickness, indicating a transition from a velocity asymmetry dominated by chiral energy to an asymmetry governed by the chiral dissipation.

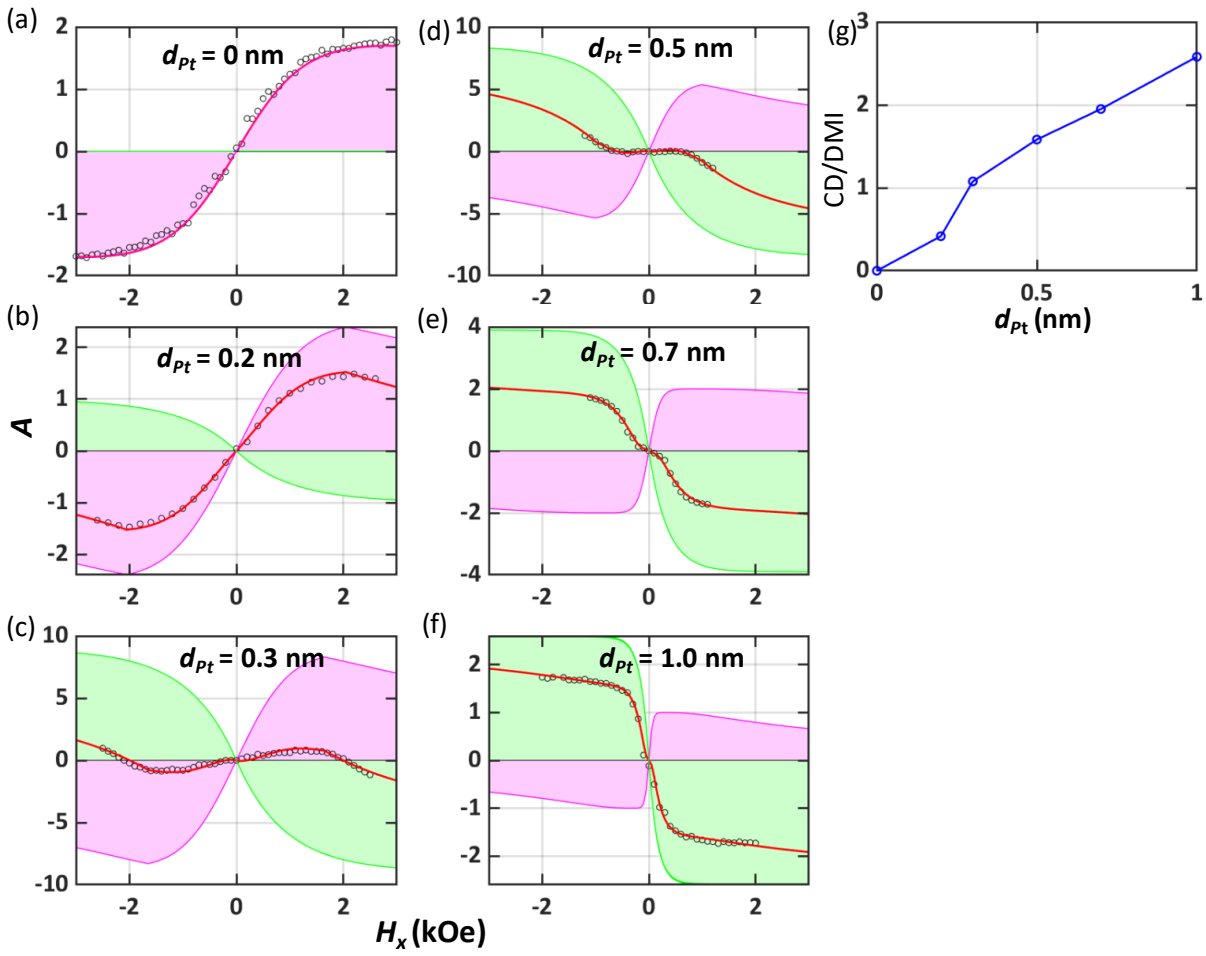

Figure 5: (a-f) In-plane field dependent asymmetry curves fitted as a combination of DMI (purple) and chiral damping (green) contribution and (g) The ratio of chiral damping and DMI (*i.e.* weight factor ratio) contributing to the asymmetry for different Pt thicknesses.

Angle dependence of velocity

To complete this study, we analyze the shape of the magnetic bubbles for various Pt thicknesses. Figure 6(a) shows bubble expansion in a sample with d_{Pt}=0 nm (left) and 1 nm (right) under the same field configuration. Based on the analysis provided above, these two samples correspond to different asymmetry mechanism: the former is dominated by DMI, while the latter is dominated by chiral damping. We immediately observe that the asymmetric bubble expansion in these two regimes is not only opposite but also present quite a different shape. To further analyze this behavior, we study the domain wall velocity as a function of angle θ, with respect to the in-plane

field. First, a circular bubble is created by an out-of-plane field and then it is expanded infinitesimally with a short out-of-plane field pulse in presence of an in-plane field. From the differential image shown in Fig. 6(b), displacements at different θ are obtained and summarized in Fig. 6(c-e). For an infinitesimal expansion, the magnetization vector at a certain θ does not change significantly. Thus, the distance measured at an angle θ corresponds to the displacement of a particular magnetization vector at boundary during expansion. Images in Fig. 6(b) correspond to the Pt thickness d_{Pt}=0, 0.5 and 1 nm (top, middle and bottom panels) at three different fields H_x=0.5, 1 and 1.5 kOe (left, central and right panels). For d_{Pt}=0 nm the expansion is favored on the right side, for d_{Pt}=0.5 nm it is more or less symmetric and for d_{Pt}=1nm it expands mostly on the left side. Figure 6(c-e) shows normalized polar plot of domain wall velocity as a function of θ at three different H_x, 0.5kOe, 1 kOe and 1.5 kOe (top, middle and bottom panels). Here we clearly see two distinct natures of θ dependence curve for d_{Pt}=0 nm (red) and d_{Pt}=1nm (magenta). For d_{Pt} =1 nm (magenta), the displacement is more sensitive to θ, resulting a sharp structure at 180° whereas for d_{Pt}=0 nm (red) the change in displacement is more gradual giving rise to a flatter curve having maxima at 0°. For d_{Pt} =0.5 (blue), we see a superposition of these two patterns. At lower field, H_x=0.5kOe the curve is more similar to d_{Pt}=0 nm, while with increasing field the curve starts having more similarities with d_{Pt}=1nm. From this observation, we can speculate, in line with the above discussion, that the two distinct angular dependence patterns at d_{Pt}=0 and 1 nm establish the fact that the asymmetry stems from two fundamentally different phenomena. Now we can identify that the flatter variation is a conscience of the energy related asymmetry and the sharp variation corresponds to the chiral damping. At 0.5 nm both the phenomena are contributing to the opposite asymmetry and thus the superposition effect is observed in angular dependence curve.

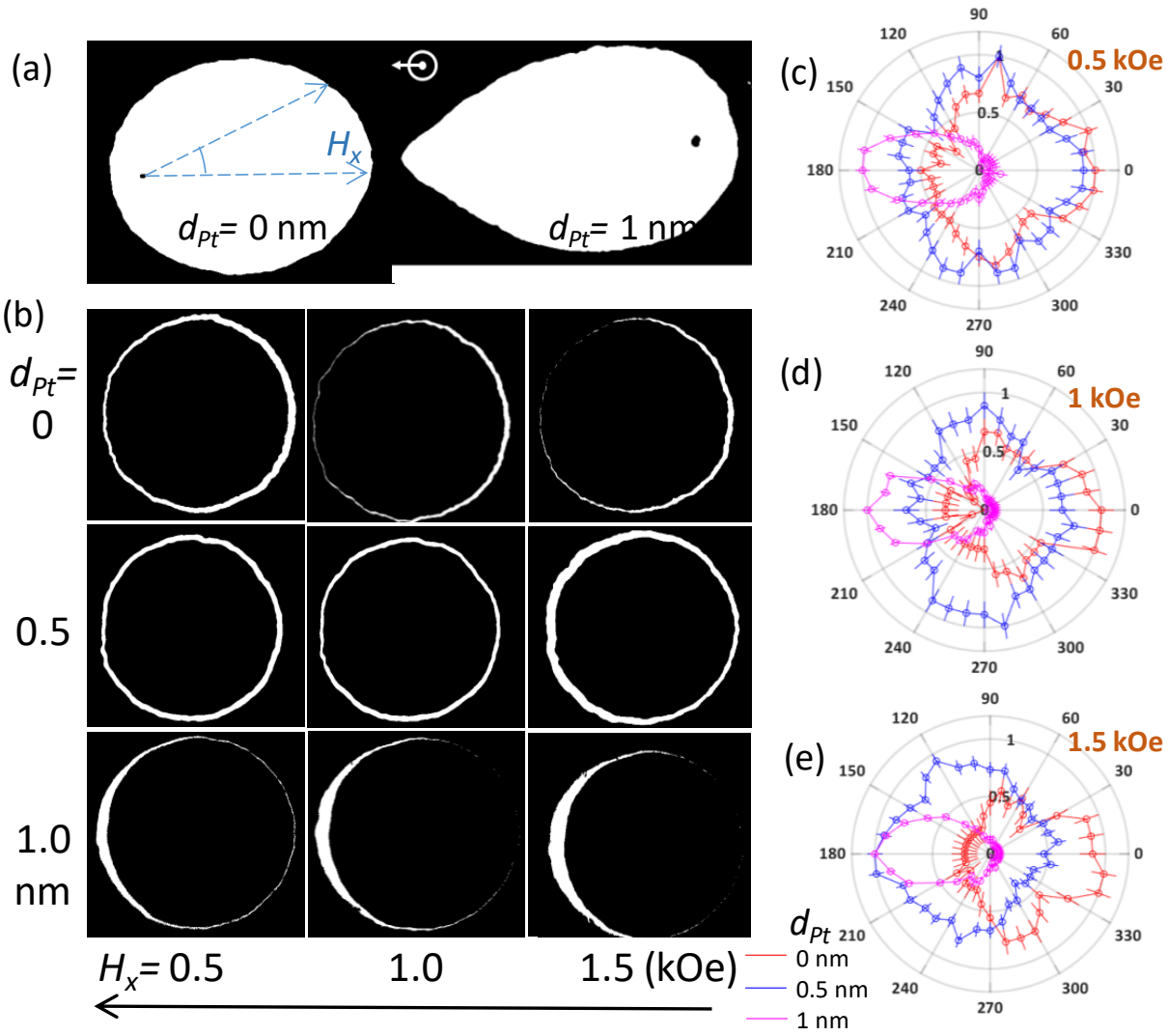

305

306 **Figure 6:** (a) The shape of bubbles for d_{Pt}=0 and 1 nm for the same field configuration, (b) Differential
307 Kerr image of small expansion of a circular bubble for different d_{Pt} at different values of H_x and (c-e)
308 show the angular displacements of bubbles corresponding to the in-plane fields 0.5, 1 and 1.5kOe. Red,
309 blue and magenta curves correspond to top Pt thickness of 0, 0.5 and 1nm respectively.

310 **Conclusions**

311 In summary, we systematically study field-driven bubble expansion in structure lacking inversion
312 symmetry. In such samples magnetic bubbles expand asymmetrically in presence of in-plane and
313 out-of-plane field. The velocity of the domain wall in the creep regime can be well fitted by the
314 creep scaling law. The velocity asymmetry can occur along or opposite to the field direction
315 depending on the domain wall chirality and DMI of the sample. Damping and energy are the most
316 important factors which control the asymmetry. Energy related asymmetry corresponds to a change

in slope while chiral damping asymmetry can be identified through a vertical shift in the out-of-plane velocity curve. In this study the velocity asymmetry is investigated in Ta(5 nm)/Pt(3 nm)/Co (0.6 nm)/IrMn(3 nm) by systematically inserting thin layer of Pt between Co and IrMn interface. The thickness of Pt varies from 0 to 1 nm. With no Pt, the asymmetry is dominated by energy having a strong effective internal field. As Pt thickness increases the internal field starts to disappear while at the same time chiral damping appears taking a leading role on asymmetry. The chiral damping asymmetry acts opposite to the energy asymmetry. As a result of these two competing effects, the asymmetry reversal occurs with increasing Pt thickness. The study is helpful for the effective control of magnetic bubbles which can be used for future memory and logic based applications.

Methods

Sample preparation: Thin film multilayer of Ta(5 nm)/Pt(3 nm)/Co (0.6 nm)/Pt(d_{Pt})/IrMn(3 nm) with d_{Pt} ranging from 0 to 5 nm were deposited on thermally oxidized Si substrates using Singulus dc/rf magnetron sputtering. The sputtering conditions were carefully chosen to obtain perpendicular magnetic anisotropy in these films. The patterned strip tracks and the electrodes are prepared using lithography and Ar-ion milling.

MOKE measurements: The experiment was performed using magneto-optical Kerr effect (MOKE) microscopy in polar geometry[42-45]. To observe the domains differential Kerr imaging was performed which helped us to eliminate nonmagnetic intensities from the image. Square pulses of the magnetic field were applied both in the plane and out-of-plane of the sample using two independent electromagnets. To nucleate a bubble, the thin film magnetization was saturated in one perpendicular direction followed by an out-of-plane field pulse in the opposite direction. The bubbles nucleate from defects or pinning centers present in the sample. An in-plane field alone cannot nucleate or drive bubbles because of strong PMA but combined with out-of-plane field it induces asymmetric motion. To ensure a proper synchronization and temporal overlap between the fields, in-plane pulse is chosen longer than the out-of-plane pulse.

Acknowledgements

AG gratefully acknowledge financial support from Khalifa University, UAE and PSE Division, KAUST, Saudi Arabia. In addition, NS, DA, and GD acknowledge the support from Khalifa University, UAE for this work.

REFERENCES:

[1] S. S. Parkin, M. Hayashi ,L. Thomas, *Science* **2008**, 320, 190-194.
[2] A. Fert, V. Cros ,J. Sampaio, *Nature nanotechnology* **2013**, 8, 152-156.
[3] M. Hayashi, L. Thomas, R. Moriya, C. Rettner ,S. S. Parkin, *Science* **2008**, 320, 209-211.
[4] S.-i. Iwasaki, *IEEE Transactions on Magnetics* **1980**, 16, 71-76.
[5] S. Khizroev, M. Kryder, Y. Ikeda, K. Rubin, P. Arnett, M. Best ,D. Thompson, *IEEE transactions on magnetics* **1999**, 35, 2544-2546.
[6] S. Piramanayagam, *Journal of Applied Physics* **2007**, 102, 2.
[7] I. M. Miron, T. Moore, H. Szambolics, L. D. Buda-Prejbeanu, S. Auffret, B. Rodmacq, S. Pizzini, J. Vogel, M. Bonfim ,A. Schuhl, *Nature materials* **2011**, 10, 419-423.
[8] T. A. Moore, I. Miron, G. Gaudin, G. Serret, S. Auffret, B. Rodmacq, A. Schuhl, S. Pizzini, J. Vogel ,M. Bonfim, *Applied Physics Letters* **2008**, 93, 262504.
[9] S.-H. Yang, K.-S. Ryu ,S. Parkin, *Nature nanotechnology* **2015**, 10, 221.
[10] Y. Zhang, W. Zhao, D. Ravelosona, J.-O. Klein, J. Kim ,C. Chappert, *Journal of Applied Physics* **2012**, 111, 093925.
[11] V. Jeudy, A. Mougin, S. Bustingorry, W. S. Torres, J. Gorchon, A. B. Kolton, A. Lemaître ,J.-P. Jamet, *Physical review letters* **2016**, 117, 057201.
[12] E. Jué, A. Thiaville, S. Pizzini, J. Miltat, J. Sampaio, L. Buda-Prejbeanu, S. Rohart, J. Vogel, M. Bonfim ,O. Boulle, *Physical Review B* **2016**, 93, 014403.
[13] I. M. Miron, G. Gaudin, S. Auffret, B. Rodmacq, A. Schuhl, S. Pizzini, J. Vogel ,P. Gambardella, *Nature materials* **2010**, 9, 230-234.
[14] S. Pizzini, J. Vogel, S. Rohart, L. Buda-Prejbeanu, E. Jué, O. Boulle, I. M. Miron, C. Safeer, S. Auffret ,G. Gaudin, *Physical review letters* **2014**, 113, 047203.
[15] M. L. Jablonski, S. Liu, C. R. Winkler, A. R. Damodaran, I. Grinberg, L. W. Martin, A. M. Rappe ,M. L. Taheri, *ACS applied materials & interfaces* **2016**, 8, 2935-2941.
[16] A. Thiaville, S. Rohart, É. Jué, V. Cros ,A. Fert, *EPL (Europhysics Letters)* **2012**, 100, 57002.
[17] S. Emori, U. Bauer, S.-M. Ahn, E. Martinez ,G. S. Beach, *Nature materials* **2013**, 12, 611-616.
[18] A. Ganguly, K. Kondou, H. Sukegawa, S. Mitani, S. Kasai, Y. Niimi, Y. Otani ,A. Barman, *Applied Physics Letters* **2014**, 104, 072405.
[19] S. Husain, X. Chen, R. Gupta, N. Behera, P. Kumar, T. Edvinsson, F. Garcia-Sanchez, R. Brucas, S. Chaudhary ,B. Sanyal, *Nano letters* **2020**, 20, 6372-6380.
[20] A. Ganguly, S. Azzawi, S. Saha, J. King, R. Rowan-Robinson, A. Hindmarch, J. Sinha, D. Atkinson ,A. Barman, *Scientific reports* **2015**, 5, 1-8.
[21] M. Grinolds, M. Warner, K. De Greve, Y. Dovzhenko, L. Thiel, R. L. Walsworth, S. Hong, P. Maletinsky ,A. Yacoby, *Nature nanotechnology* **2014**, 9, 279.
[22] L. Rondin, J.-P. Tetienne, P. Spinicelli, C. Dal Savio, K. Karrai, G. Dantelle, A. Thiaville, S. Rohart, J.-F. Roch ,V. Jacques, *Applied Physics Letters* **2012**, 100, 153118.
[23] J. R. Maze, P. L. Stanwix, J. S. Hodges, S. Hong, J. M. Taylor, P. Cappellaro, L. Jiang, M. G. Dutt, E. Togan ,A. Zibrov, *Nature* **2008**, 455, 644-647.

[24] S. Finizio, S. Wintz, K. Zeissler, A. V. Sadovnikov, S. Mayr, S. A. Nikitov, C. H. Marrows ,J. r. Raabe, *Nano letters* **2018**, 19, 375-380.
[25] D. Shindo ,Y. Murakami, *Journal of Physics D: Applied Physics* **2008**, 41, 183002.
[26] E. Snoeck, C. Gatel, L. Lacroix, T. Blon, S. Lachaize, J. Carrey, M. Respaud ,B. Chaudret, *Nano letters* **2008**, 8, 4293-4298.
[27] A. Tonomura, T. Matsuda, J. Endo, T. Arii ,K. Mihama, *Physical Review Letters* **1980**, 44, 1430.
[28] L. A. Turnbull, M. T. Birch, A. Laurenson, N. Bukin, E. O. Burgos-Parra, H. Popescu, M. N. Wilson, A. Stefančič, G. Balakrishnan ,F. Y. Ogrin, *ACS nano* **2020**.
[29] Y. P. Ivanov, A. Chuvilin, S. Lopatin, H. Mohammed ,J. Kosel, *ACS applied materials & interfaces* **2017**, 9, 16741-16744.
[30] H. S. Park, J. S. Baskin ,A. H. Zewail, *Nano letters* **2010**, 10, 3796-3803.
[31] X. Yu, J. P. DeGrave, Y. Hara, T. Hara, S. Jin ,Y. Tokura, *Nano letters* **2013**, 13, 3755-3759.
[32] K. Shibata, T. Tanigaki, T. Akashi, H. Shinada, K. Harada, K. Niitsu, D. Shindo, N. Kanazawa, Y. Tokura ,T.-h. Arima, *Nano letters* **2018**, 18, 929-933.
[33] S. Zhang, J. Zhang, Y. Wen, E. M. Chudnovsky ,X. Zhang, *Communications Physics* **2018**, 1, 1-7.
[34] G. Gubbiotti, S. Tacchi, M. Madami, G. Carlotti, A. Adeyeye ,M. Kostylev, *Journal of Physics D: Applied Physics* **2010**, 43, 264003.
[35] M. Madami, S. Bonetti, G. Consolo, S. Tacchi, G. Carlotti, G. Gubbiotti, F. Mancoff, M. A. Yar ,J. Åkerman, *Nature nanotechnology* **2011**, 6, 635.
[36] T. Sebastian, K. Schultheiss, B. Obry, B. Hillebrands ,H. Schultheiss, *Frontiers in Physics* **2015**, 3, 35.
[37] A. Cao, X. Zhang, B. Koopmans, S. Peng, Y. Zhang, Z. Wang, S. Yan, H. Yang ,W. Zhao, *Nanoscale* **2018**, 10, 12062-12067.
[38] A. Hrabec, N. Porter, A. Wells, M. Benitez, G. Burnell, S. McVitie, D. McGrouther, T. Moore ,C. Marrows, *Physical Review B* **2014**, 90, 020402.
[39] Y. Iunin, Y. P. Kabanov, V. Nikitenko, X. Cheng, D. Clarke, O. Tretiakov, O. Tchernyshyov, A. Shapiro, R. Shull ,C. Chien, *Physical review letters* **2007**, 98, 117204.
[40] E. Jué, C. Safeer, M. Drouard, A. Lopez, P. Balint, L. Buda-Prejbeanu, O. Boulle, S. Auffret, A. Schuhl ,A. Manchon, *Nature materials* **2016**, 15, 272-277.
[41] K. Shahbazi, J.-V. Kim, H. T. Nembach, J. M. Shaw, A. Bischof, M. D. Rossell, V. Jeudy, T. A. Moore ,C. H. Marrows, *Physical Review B* **2019**, 99, 094409.
[42] P. Chvykov, V. Stoica ,R. Clarke, *arXiv preprint arXiv:1212.3259* **2012**.
[43] M. Cormier, J. Ferré, A. Mougin, J.-P. Cromières ,V. Klein, *Review of Scientific Instruments* **2008**, 79, 033706.
[44] I. Soldatov ,R. Schäfer, *Journal of Applied Physics* **2017**, 122, 153906.
[45] S. Zhang, X. Zhang, J. Zhang, A. Ganguly, J. Xia, Y. Wen, Q. Zhang, G. Yu, Z. Hou ,W. Wang, *Science advances* **2020**, 6, eaay1876.
[46] F. Ajejas, A. Gudín, R. Guerrero, A. Anadon Barcelona, J. M. Diez, L. de Melo Costa, P. Olleros, M. A. Niño, S. Pizzini ,J. Vogel, *Nano letters* **2018**, 18, 5364-5372.
[47] W. Wang, Y.-F. Zhao, F. Wang, M. W. Daniels, C.-Z. Chang, J. Zang, D. Xiao ,W. Wu, *Nano Letters* **2021**, 21, 1108-1114.
[48] J. Yu, X. Qiu, Y. Wu, J. Yoon, P. Deorani, J. M. Besbas, A. Manchon ,H. Yang, *Scientific reports* **2016**, 6, 1-9.
[49] A. W. Wells, P. M. Shepley, C. H. Marrows ,T. A. Moore, *Physical review B* **2017**, 95, 054428.
[50] F. Ajejas, V. Křižáková, D. de Souza Chaves, J. Vogel, P. Perna, R. Guerrero, A. Gudin, J. Camarero ,S. Pizzini, *Applied Physics Letters* **2017**, 111, 202402.
[51] P. Kuświk, M. Matczak, M. Kowacz, K. Szuba-Jabłoński, N. Michalak, B. Szymański, A. Ehresmann ,F. Stobiecki, *Physical Review B* **2018**, 97, 024404.

436 [52] P. Chauve, T. Giamarchi ,P. Le Doussal, *Physical Review B* **2000**, 62, 6241.

437